Monografías Matemáticas *García de Galdeano* **39**, 45–55 (2014)

AN ADAPTIVE NXFEM FOR THE INTERFACE PROBLEM

Nelly Barrau, Roland Becker, Eric Dubach and Robert Luce

Abstract. We propose an adaptive finite element method for the elliptic interface problem with piecewise constant coefficients, based on a robust variant of the original NXFEM of Hansbo and Hansbo [5]. This method takes into account discontinuities that are not necessarily aligned with the mesh. Our robust variant [2], introducing pondaration coefficients, provides constants in the error estimates which are independent both of the geometry of the cut cells and of the coefficients. Suitable error estimators have been derived in [1]. In this paper, we extend the method to quadrilateral meshes and describe numerical implementation.

Keywords: Elliptic interface problem, NXFEM, adaptive methods, a posteriori error estimates.

AMS classification: 65N30, 65N50, 76M10.

§1. Introduction

We propose an adaptive finite element method for the interface problem in a two-dimensional domain

$$\begin{aligned} \operatorname{div}(\sigma) = f \quad \text{in } \Omega, \quad \sigma = -k\nabla u, \\ u = 0 \quad \text{on } \partial\Omega. \end{aligned} \tag{1.1}$$

Let Ω be a polygonal domain, with convex polygonal boundary $\partial\Omega$ and an internal smooth boundary Γ dividing Ω into two open sets Ω_{in} and Ω_{ex} (see Figure 1).

For simplicity, we suppose k to be a piecewise constant discontinuous coefficient taking values k_{in} and k_{ex} on the two disjoint subdomains Ω_{in} and Ω_{ex} and $f \in L^2(\Omega)$.

The discretization of (1.1) is based on the Nitsche extended finite element method (NXFEM). For the interface problem developed in [5], the method uses standard finite element spaces on either side of the discontinuity and weak conditions along Γ. The finite element space is obtained by 'doubling' of the local functions space on all cut cells by the interface Γ, which is here assumed to be polygonal.

The discontinuity of the discrete functions is handled by a variant of Nitsche's method [6], making use of the interface conditions

$$[u] = 0 \quad \text{and} \quad [\sigma \cdot n] = 0 \quad \text{on } \Gamma,$$

where n is the unit outer normal field of Ω_{in}. We refer to [5] where the stability of the method and optimal order error estimates have been obtained, supposing only that the solution is piecewise in H^2.

In [2] we have proposed a robust variant of the original method on triangular meshes, introducing a weighting taking into account not only the geometry of the cut cells, but also the

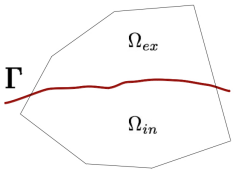

Figure 1: Notations.

coefficients. The resulting method coincides on matching meshes with the weighted discontinuous Galerkin method of Ern and Stephanson [4]. In [1] we have proposed an *a posteriori* error estimator based on the evaluation of cell- and edge-wise residuals for triangular meshes, resulting in an adaptive algorithm of the classical form

$$\text{Solve} \longrightarrow \text{Estimate} \longrightarrow \text{Mark} \longrightarrow \text{Refine}.$$

Throughout, we use the symbol $\lesssim$ to indicate that an inequality holds with constants independent of any geometrical parameter and the values of the coefficient k.

Here we explain the method and the implementation on quadrilateral meshes.

§2. Knowledges on triangular meshes

We denote by $\mathcal{H}$ a family of uniformly shape-regular meshes h consisting of triangles $\mathcal{K}_h$. We define the set of cut cells by

$$\mathcal{K}_h^{\text{in}} := \{K \cap \Omega_{\text{in}} : K \in \mathcal{K}_h \text{ such that } K \cap \Omega_{\text{in}} \neq \emptyset\},$$

and similarly for $\mathcal{K}_h^{\text{ex}}$. Let $\mathcal{K}_h^{\text{cut}} := \mathcal{K}_h^{\text{in}} \cup \mathcal{K}_h^{\text{ex}}$. In addition we denote by $\mathcal{K}_h^*$ the set of all uncut cells augmented by $\mathcal{K}^{\text{cut}}$. We then define the finite element spaces

$$V := \{v \in L^2(\Omega) : v \in C(\Omega),\ v|_K \in P^1(K)\ \forall K \in \mathcal{K}_h\},$$

and

$$\mathbb{V}_h := \left\{v_h \in L^2(\Omega) : v_h|_{\Omega_{\text{in}}} \in C(\Omega_{\text{in}}),\ v_h|_{\Omega_{\text{ex}}} \in C(\Omega_{\text{ex}}),\ v_h|_M \in P^1(M)\ \forall M \in \mathcal{K}_h^{\text{cut}}\right\}.$$

The functions of $\mathbb{V}_h$ are discontinuous across the interface (see Figure 2) which is divided into the set of segments

$$\mathcal{S}_h^\Gamma := \{K \cap \Gamma : K \in \mathcal{K}_h \text{ such that } K \cap \Gamma \neq \emptyset\}.$$

Let $v_h \in \mathbb{V}_h$. For a given interior side $S \in \mathcal{S}_h^\Gamma$ we fix a unit normal n_S once for all and define for $x \in S$

$$v_{h_S}^{\text{in}}(x) := \lim_{\varepsilon \searrow 0} v_h(x - \varepsilon n_S), \quad v_{h_S}^{\text{ex}}(x) := \lim_{\varepsilon \searrow 0} v_h(x + \varepsilon n_S).$$

Next we define the jump and weighted mean for a weight $0 \leq \alpha \leq 1$ by

$$[u](x) := u_S^{\text{in}}(x) - u_S^{\text{ex}}(x), \quad \{u\}_\alpha(x) := \alpha u_S^{\text{in}}(x) + (1-\alpha) u_S^{\text{ex}}(x).$$

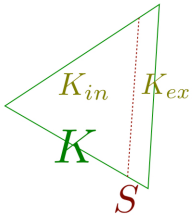

Figure 2: A cut triangle.

The following formula readily follows from these definitions:

$$[uv] = [u]\{v\}_\alpha + \{u\}_{1-\alpha}[v],$$

We define the linear functional

$$l(v_h) = \int_\Omega f v_h + \int_{\mathcal{S}_h^\Gamma} g_N \{v_h\}_{1-\alpha} \tag{2.1}$$

and the symmetric bilinear form

$$a_h(u_h, v_h) = \sum_{M \in \mathcal{K}_h^{\text{in}} \cup \mathcal{K}_h^{\text{ex}}} \int_M k \nabla u_h \cdot \nabla v_h - \sum_{S \in \mathcal{S}_h^\Gamma} \int_S \left([u_h] \partial_{n,k}^* v_h + \partial_{n,k}^* u_h [v_h] \right), \tag{2.2}$$

where we have used the discrete fluxes

$$\partial_{n,k}^* v_h|_S := \{\partial_{n,k} v_h\}_{\alpha_S} - \gamma_S [v_h] \quad (\partial_{n,k} v_h := n_S^T k \nabla v_h),$$

which depend on the two parameters α_S and γ_S, defined as

$$\alpha_S := \frac{k_{\text{ex}}|K^{\text{in}}|}{k_{\text{ex}}|K^{\text{in}}| + k_{\text{in}}|K^{\text{ex}}|}, \qquad \gamma_S := \gamma_0 \frac{k_{\text{in}}\, k_{\text{ex}}\, |S|}{k_{\text{ex}}|K^{\text{in}}| + k_{\text{in}}|K^{\text{ex}}|},$$

with $\gamma_0 > 0$ depending on the polynomial degree but neither on the diffusion coefficients nor the mesh geometry [2].

We define the energy-type norm

$$|||v_h|||_h^2 := \left\| k^{1/2} \nabla v_h \right\|^2 + \|v_h\|_{h,\Gamma}^2, \quad \|v_h\|_{h,\Gamma}^2 := \sum_{S \in \mathcal{S}_h^\Gamma} \gamma_S \, \|[v_h]\|^2$$

We are interested in reducing the error

$$e_h := \left(\left\| k^{1/2} \nabla (u - u_h) \right\|^2 + \|u_h\|_{h,\Gamma}^2 \right)^{1/2}. \tag{2.3}$$

The main difficulty induced by NXFEM with respect to continuous FEM is the nonconformity caused by the doubling of the unknowns on the interface cells. As usual in non-conforming methods, we therefore introduce the projection on the continuous space.

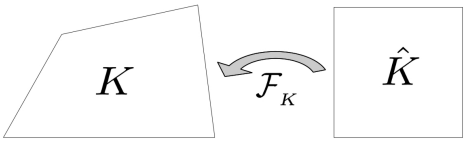

Figure 3: Classical quadrilateral mapping.

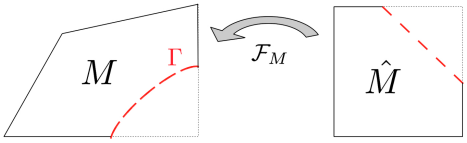

Figure 4: Partial quadrilateral mapping.

We define the cell contribution of the estimator [1]

$$\eta_h(K) := \left(\frac{|K|^2}{k} \|\pi_K f + \operatorname{div}(k\nabla u_h)\|_K^2 + \sum_{S\subset\partial K^*} \frac{|S|}{k} \left\|[\partial_{n,k} u_h]\right\|_S^2 + \sum_{S\in\mathcal{S}_h^\Gamma} \left(\frac{1}{\gamma_S} \left\|[\partial_{n,k} u_h]\right\|_S^2 + \gamma_S \|[u_h]\|_S^2 \right) \right)^{1/2}, \tag{2.4}$$

where π_K is the $L^2(K)$-projection on the constants and $\partial K^* := \partial K \setminus \partial\Omega$. Next, we introduce a data-approximation estimator

$$\mu_h(K) := |K|^{1/2} \|f - \pi_K f\|_K, \quad \mu_h(\mathcal{M}) := \left(\sum_{K\in\mathcal{M}} \mu_h(K)^2 \right)^{1/2}.$$

Combination of Lemma in [1] yields

Theorem 1. *We have the following upper bound*

$$e_h^2 \lesssim \eta_h^2(\mathcal{K}_h^*) + \mu_h^2(\mathcal{K}_h^*),$$

with contents independent of the mesh geometry and k.

§3. On quadrilateral meshes

3.1. Definition of the method

Now we consider a regular family of quadrilateral meshes $\mathcal{H}$. As for triangular meshes, we assume that the interface intersects each element boundary ∂K exactly twice, and each (open) edge at most once. Notation employed here are described in Section 2. Moreover, the classical notations for continuous quadrilateral FE of degree 1 will be used.

We note (cf. Figure 3):

- K current element,
- $\hat{K} = [-1, 1]^2$ the reference element,
- $\mathcal{F}_K$ a Q^1-mapping[1] from $\hat{K}$ to K.

In addition, for all $M \subset K$, we note $\hat{M} = \mathcal{F}_K^{-1}(M)$ and $\mathcal{F}_M = \mathcal{F}_K|_{\hat{M}}$ (cf. Figure 4).

[1] We remark that a Q^1-mapping is bilinear, while a P^1-mapping is affine.

Figure 5: Split by Γ into two polygons.

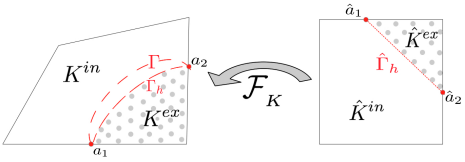

Figure 6: The interface was copied on $\hat{K}$.

The finite element space is now defined as the isoparametric space

$$\mathbb{V}_h := \{v_h \in L^2(\Omega) : v_h|_{\Omega_{\text{in}}} \in C(\Omega_{\text{in}}),\ v_h|_{\Omega_{\text{ex}}} \in C(\Omega_{\text{ex}}),\ v_h|_M \circ \mathcal{F}_M \in Q^1(\hat{M})\ \forall M \in \mathcal{K}_h^{\text{cut}}\}. \quad (3.1)$$

A FE basis for $\mathbb{V}_h$ is obtained from a standard FE basis on the mesh by replacing each standard basis function living on a cut element by two new basis functions, namely its restrictions to Ω_{in} and Ω_{ex} respectively. Both these new basis functions are represented in the implementation using the same nodes[2] from the original quadrangulation.

In order to implement the discontinuous approximation, we first determined the set of quadrilaterals intersected by Γ. We assumed that a cut cell K was split by Γ into two polygons (see Figure 5).

We determine the approximation Γ_h of Γ on the cut cell K by the following steps (cf. Figure 6):

1. $\{a_1, a_2\} = \Gamma \cap \partial K$,
2. $a_i = \mathcal{F}_K(\hat{a}_i)$, for $i = 1, 2$,
3. $\hat{\Gamma}_h = [\hat{a}_1, \hat{a}_2]$,
4. $\Gamma_h = \mathcal{F}_K(\hat{\Gamma}_h)$.

The main difficulty of this approach deals with the numerical evaluation of the integral terms (see (2.2) and (2.1)) on the cut elements as well as on the discontinuity. We have got around this problem by building numerical integration formulas on each polygon and on the interface. This process enable us to use the standard assemble techniques of the finite element method.

For any $v_h \in \mathbb{V}_h$, $v_h|_{\Omega_{\text{in}}}$ is decomposed using the FE basis functions of cells covering Ω_{in}, and $v_h|_{\Omega_{\text{ex}}}$ is decomposed using those of cells covering Ω_{ex} respectively. In a cut element, v_h can be expressed using the restriction of basis functions on K^{in} and K^{ex} as follows:

$$v_h|_{K^{\text{in}}} = \sum_{i=0}^{3} \alpha_i\, \varphi_i|_{K^{\text{in}}}, \qquad v_h|_{K^{\text{ex}}} = \sum_{i=0}^{3} \alpha'_i\, \varphi_i|_{K^{\text{ex}}}. \quad (3.2)$$

So, we need eight degrees of freedom α_i and α'_i with $i = 0, \ldots, 3$ in order to define v_h on a cut cell (Figure 7).

The continuity between cut and uncut elements is guaranteed by the definitions (3.1) and (3.2). Each polygon on $\hat{K}$ was split into triangles in order to obtain interpolation formula on it.

In addition, we proceed as follows. The quadrilaterals that were not crossed by Γ (ie $K \in \mathcal{K}_h^*$) were handled in the usual way (see Figure 3). On the elements crossed by the

[2]Recall that the Q^1 degrees of freedom (dof) and the Q^1 basis functions are associated with the geometrical nodes

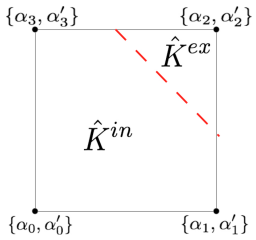

Figure 7: Dof distribution.

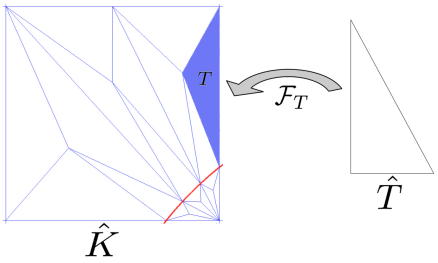

Figure 8: Independent meshes on each subdomain.

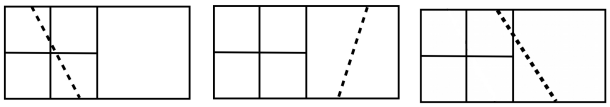

Figure 9: Cut quadrilaterals with hanging node.

interface, we have two polygons, each split into triangles. We used quadrature to evaluate all terms on the reference-reference triangle $\hat{T}$ (see Figure 8). On the interface, we used Gaussian quadrature.

3.2. Adaptive algorithm and hanging nodes

Now we consider the family of locally refined quadrilateral meshes $\mathcal{H}$ with hanging nodes. We impose on the refinement algorithm the condition that at most one hanging node is present on each edge. It can be achieved by additional bisection of cells, without destroying the overall linear complexity of the refinement algorithm, see [3].

The definition of $\mathbb{V}_h$ (3.1) implies some care on the implementation in the case of cut cells neighboring a hanging node (see Figure 9).

In the first case the interface crosses a refined quadrilateral, in the second case a coarse neighbor of a refined quadrilateral and a refined quadrilateral with its coarse neighbor in the last case (Figure 9). In order to guarantee the continuity of each function v_h in $\mathbb{V}_h$ on Ω_{in} and Ω_{ex}, we use linear interpolation for the hanging node.

To determine the nodal value corresponding to the hanging node, according its location in Ω, we only use the degree of freedom of v_h associated to the same subdomain.

The resulting method is uniformly stable with respect to the geometry of the cut cells and diffusion parameter.

The *a posteriori* error estimator is identical to the case of triangular meshes and it can be verified that Theorem 1 holds true.

§4. Implementation

Several numerical tests have been performed. First, the new formula's robustness and the estimator's efficiency were tested in [2] and we obtained satisfactory simulations on uniformly

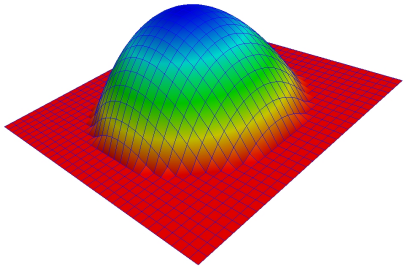

Figure 10: Configuration.

refined triangular and quadrilateral meshes [1]. We considered a two-dimensional example (from [5]). The exact solution is given by:

$$u(x,y) = \begin{cases} \dfrac{r^2}{k_{\text{in}}}, & \text{if } r \le r_0, \\ \dfrac{r^2 - r_0^2}{k_{\text{ex}}} + \dfrac{r_0^2}{k_{\text{in}}}, & \text{else,} \end{cases} \tag{4.1}$$

with

- $r := \sqrt{x^2 + y^2}$, with $r_0 = 0.75$,
- $\Omega =]-1, 1[\times]-1, 1[$,
- $k_{\text{in}} = 1$, $k_{\text{ex}} = 1000$,
- $f = -4$,
- Dirichlet boundary condition.

4.1. Uniform refinement

We use continuous quadrilateral FE of degree 1. Recall that the residual error estimator η_h is defined in (2.4) and the error in energy norm e_h in (2.3). We refer to [1] for the convergence's table and curves of a uniform refinement on cartesian quadrilateral mesh. We concluded that the estimator and the error have the same behavior as for uniform refinement on triangular mesh.

He propose here to confirm these findings, by testing the interface problem (4.1) on deformed quadrilateral meshes.

Note that the standard refinement procedure —which consists of refining by joining the sides middle— creates successive meshes in which all elements tend to parallelograms. The transformation $\mathcal{F}_K$ becomes also affine. In order to maintain deformed quadrilateral meshes on each level of refinement, we have geared down the same pattern.

Figure 11 shows these various patterns that have been used, and the convergence curves of the *REstimator* η_h and the *ENorm* e_h that we obtained on these meshes are presented in Figure 12. These reassure our previous findings.

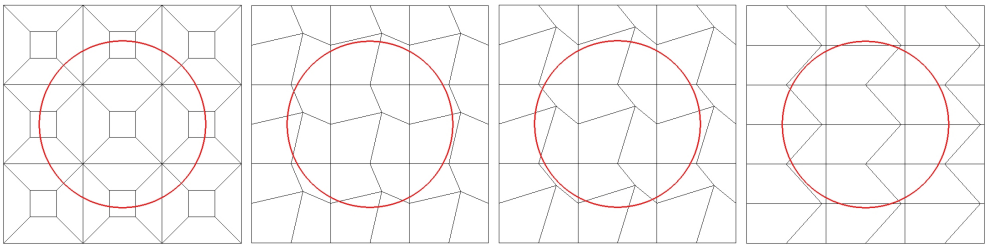

(a) Distortion 1 (b) Distortion 2 (c) Distortion 3 (d) Distortion 4

Figure 11: Deformed quadrilateral meshes.

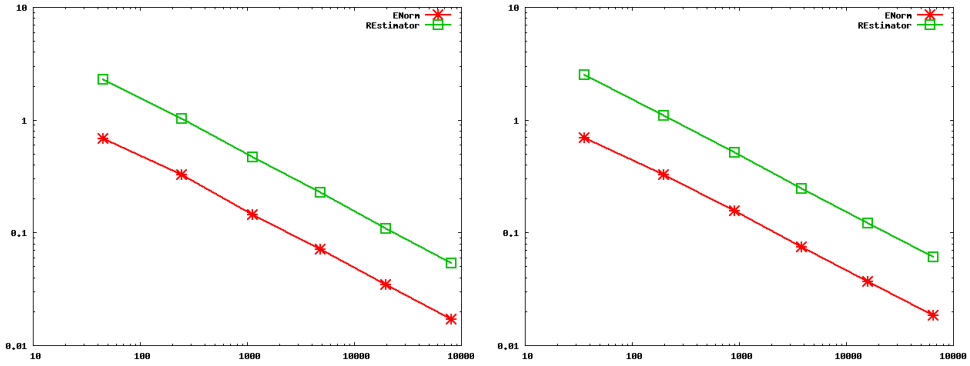

(a) Distortion 1 (b) Distortion 2

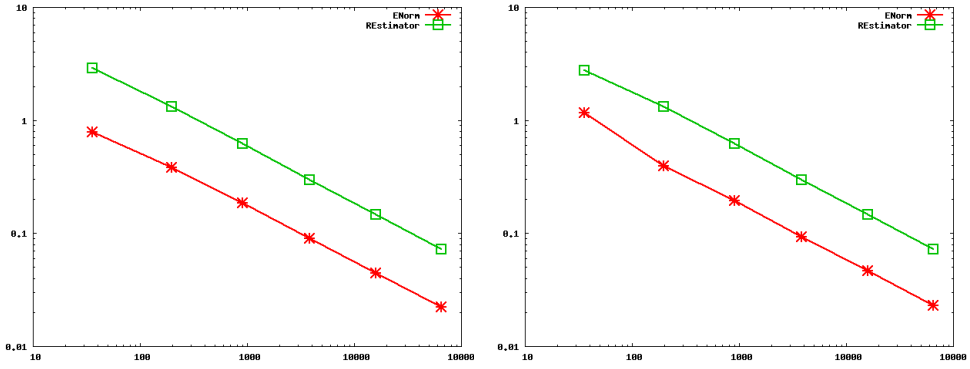

(c) Distortion 3 (d) Distortion 4

Figure 12: Convergence curves of uniform refinement on deformed quadrilateral meshes.

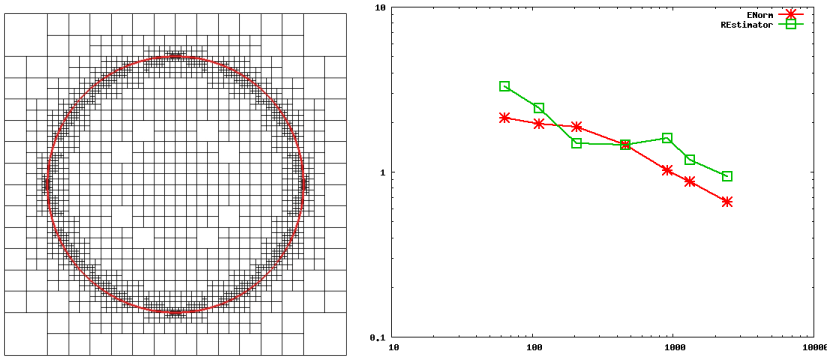

(a) Mesh (2428 elements) (b) Convergence curves

Figure 13: Adaptive refinement with classical FEM.

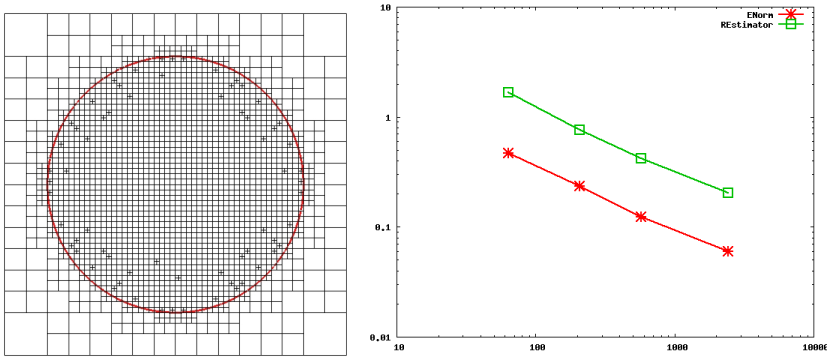

(a) Mesh (2428 elements) (b) Convergence curves

Figure 14: Adaptive refinement with NXFEM.

4.2. Adaptive refinement

The model problem (4.1) that we took has no singularity. Therefore, the estimator should mark the cells on which the solution has as many variations.

The pictures in Figure 13 show an adaptive refinement on cartesian quadrilateral mesh, using classical FEM. While when using this method, the adaptive procedure concentrates the refinement around the discontinuity (see Figure 13(a)) because the fluxes are not correctly approximated on the cut cells. The convergence curves in Figure 13(b) confirm this analysis.

When we use NXFEM and the estimator (2.4) to adapt the mesh, the normal derivatives are well approximated on the cut cells. Therefore the mesh is uniformly refined on Ω_{in} (as shown in Figure 14(a)). We find the same convergence order (see Figure 14(b)) for the uniform refinement on triangular and quadrilateral meshes, and for adaptive refinement on triangular meshes [1].

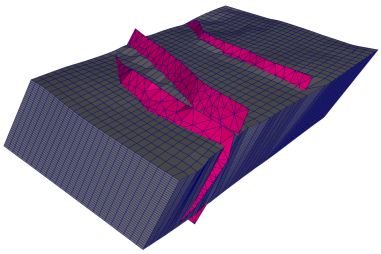

Figure 15: Configuration example in porous media problems.

§5. Evolution

To date, many opportunities are available, some of which are underway.

The procedure described in Section 3.1 can be extended significantly. In a first time, we are currently completing its generalization to finite elements of degree k on triangular, quadrilateral and hexahedral meshes.

We would essentially guide our work towards industrial applications. We would so test the method on:

- convection problems,
- time-dependant problems,
- varying the discontinuity's width (thickness),
- varying the discontinuity's number...

These configurations are commonly encountered in porous media problems (Black oil model, reservoir meshes for example, see Figure 15), but also at the microscopic level, in order to take into account, for example, the mobility and flexibility of the cells. We stand at the microscopic level in order to take into account the mobility and/or flexibility of the cells —such as red blood cells or bacteria— under the action of a liquid flow such as plasma or biofilm.

References

[1] Barrau, N., Becker, R., Dubach, E., and Luce, R. An adaptive nxfem for the interface problem on locally refined triangular and quadrilateral meshes. In *European Congress on Computational Methods in Applied Sciences and Engineering (ECCOMAS)* (2012), J. e. e. Eberhardsteiner, Ed.

[2] Barrau, N., Becker, R., Dubach, E., and Luce, R. A robust variant of nxfem for the interface problem. *C. R. Math. Acad. Sci. Paris 350* (2012), 789–792.

[3] Bonito, A., and Nochetto, R.-H. Quasi-optimal convergence rate of an adaptive discontinuous galerkin method. *SIAM J. Numer. Anal. 48* (2010), 734–771.

[4] Ern, A., Stephansen, A.-F., and Zunino, P. A discontinuous galerkin method with weighted averages for advection-diffusion equations with locally small and anisotropic diffusivity. *SIAM J. Numer. Anal. 29* (2009), 235–256.

[5] Hansbo, A., and Hansbo, P. An unfitted finite element method, based on nitsche's method, for elliptic interface problems. *Comput. Methods Appl. Mech. Eng. 191* (2002), 5537–5552.

[6] Nitsche, J. Über ein variationsprinzip zur lösung von dirichlet-problemen bei verwendung von teilräumen, die keinen randbedingungen unterworfen sind. *Abh. Math. Sem. Univ. Hamburg 36* (1971), 9–15.

LMA & Equipe Concha
UPPA - IPRA BP 1155
Avenue de l'Université
64013 PAU CEDEX - FRANCE
nelly.barrau@univ-pau.fr, roland.becker@univ-pau.fr,
eric.dubach@univ-pau.fr, robert.luce@univ-pau.fr